



## Computational vector fiducial for deflectometry system alignment

HYUKMO KANG,<sup>1</sup> HENRY QUACH,<sup>1</sup> JOEL BERKSON,<sup>1</sup> MAHAM AFTAB,<sup>1</sup> GEORGE SMITH,<sup>1</sup> HEEJOO CHOI,<sup>1,2</sup> AND DAEWOOK KIM<sup>1,2,3,\*</sup>

<sup>1</sup>Wyant College of Optical Sciences, University of Arizona, 1630 E. University Blvd., Tucson, Arizona 85721, USA

<sup>2</sup>Large Binocular Telescope Observatory, 933 N. Cherry Ave., Tucson, Arizona 85721, USA

<sup>3</sup>Department of Astronomy and Steward Observatory, University of Arizona, 933 N. Cherry Ave., Tucson, Arizona 85721, USA

\*Corresponding author: dkim@optics.arizona.edu

Received 3 September 2021; revised 4 October 2021; accepted 17 October 2021; posted 18 October 2021 (Doc. ID 442223); published 4 November 2021

**One of deflectometry's cardinal strengths is its ability to measure highly dynamically sloped optics without needing physical null references. Accurate surface measurements using deflectometry, however, require precise calibration processes. In this Letter, we introduce an alignment technique using a computational fiducial to align a deflectometry system without additional hardware equipment (i.e., algorithmic innovation). Using the ray tracing program, we build relationships between the plane of the screen and detector and algorithmically generate a fiducial pattern for the deflectometry configuration. Since the fiducial pattern is based on ideal system geometry, misalignment of the unit under test with its target position causes a discrepancy between the actual image on the camera detector and the ideal fiducial image. We leverage  $G$  and  $C$  vector polynomials to quantify misalignment and estimate the alignment status through a reverse optimization method. Simulation and experimental results demonstrate that the proposed algorithm can align the 195 mm × 80 mm of a rectangular aperture freeform optic within 10  $\mu\text{m}$  of peak-to-valley accuracy. The computational fiducial-based alignment algorithm is simple to apply and can be an essential procedure for conventional methods of deflectometry system alignment.** © 2021 Optical Society of America

<https://doi.org/10.1364/OL.442223>

The demand for freeform metrology remains commensurate with the growing demand for freeform optics in high-performance systems. Deflectometry is an attractive solution in this metrology solution space because it possesses a large dynamic slope-measuring range and does not require null optics [1,2]. These features enable a single deflectometry system to measure various types of optical surfaces without extensive changes.

Without significant effort for pre-alignment, deflectometry can measure the optics, but reliable calibration and alignment are critical for accurate surface slope measurement. To determine the positions of deflectometry system components, external measuring devices such as coordinate measuring

machines or laser trackers can be used [2,3]. Additionally, calibration techniques utilizing reference features with known surfaces [4–8], employing Zernike polynomial to analyze misalignment [9–11], or minimizing differences between model and observed geometric parameters through iterative calculation [12–14] are studied by various researchers to calibrate the deflectometry system or align optical surfaces.

In this Letter, we introduce an alignment algorithm for deflectometry systems using an inversely calculated computational fiducial and demonstrate it in both simulation and experiments. This method is analogous to an interferometer's alignment mode, which guides users to overlap two focused spots from the reference beam and the test beam. The presented algorithm leveraged  $G$  and  $C$  vector polynomials [15,16] to quantify the alignment status and calculate the misalignment using reverse optimization. Especially, the inverse ray tracing calculation creates uniformly distributed fiducial grid spots on the deflectometry camera image. This algorithmic innovation enables systematic vector polynomial fitting on the measured spots to solve the alignment problem of a non-null testing nature (e.g., configuration dependent complex sinusoidal patterns). The alignment quality was evaluated using optical testing criteria to illustrate its sensitivity and utility in metrology applications.

A deflectometry system consists of an illumination source, a unit under test (UUT), and a camera (Fig. 1). Typically a digital screen is used as the illumination source, and the camera is focused on the UUT to establish conjugate imaging between the camera detector and the UUT. By modulating the displayed phase-stepped sinusoidal patterns and calculating phase at the image detector, a pixel-to-pixel correspondence among the screen, UUT, and detector is obtained. Using the coordinate information of all associated data and the law of reflection, deflectometry calculates the local slope distribution of UUT [1].

The deflectometry ray tracing simulator [17] provides coordinate relationships among the screen, UUT, and detector pixels. This feature is used to inversely generate the computational fiducial pattern to assist alignment of the deflectometry setup. The fiducial pattern is a specific pattern displayed on the screen that maps a grid dot image onto the camera detector. In Fig. 2(a),

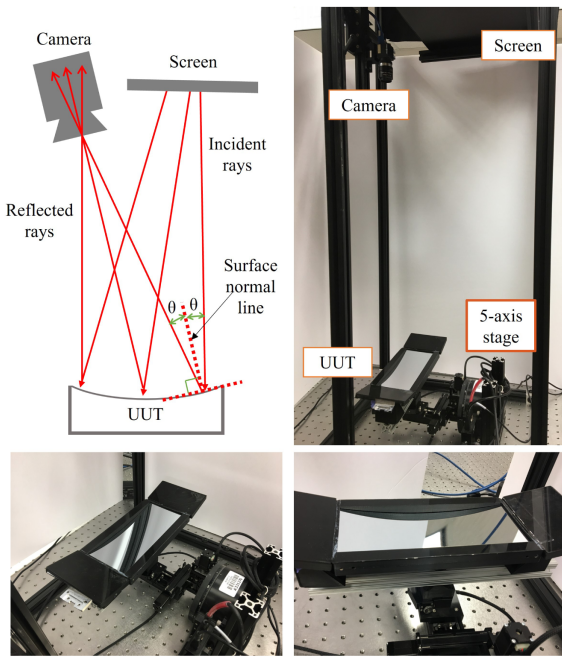


**Fig. 1.** (top left) Schematic diagram of deflectometry setup. The light source (screen) emits rays that are reflected at the UUT and collected by the camera. (top right) Experimental setup of deflectometry. (bottom left) UUT mounted on the computer-controlled rigid-body motion stage. (bottom right) Zoom-in view of the freeform UUT.

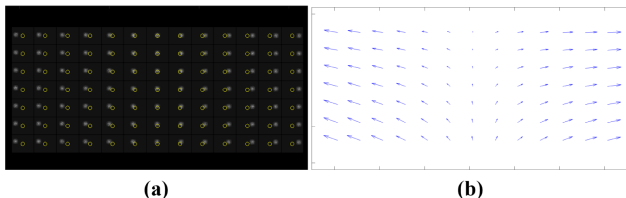


**Fig. 2.** Simulated images for computational fiducial pattern application. (a) Observed image of fiducial pattern at the detector plane. White dots are measured patterns and yellow circles are fiducial from model. (b) Vector map drawn from computational yellow circles to measured white dots, which are updated real-time.

the yellow circles are the locations of the fiducial for a perfectly aligned system, the recorded white dots mark their observed locations, and the gray squares are equally distributed areas for each zonal analysis. Each dot is 2D Gaussian shape to reduce the ambiguity in position determination. Since this pattern is calculated based on model geometry parameters, any deviation from the fiducial points implies an inconsistency in the geometry parameters between the model and the experimental setup. It is worthy to note that, if a surface shape error is in a way that it produces the same vector fiducial changes as a misalignment, such fundamental degeneracy cannot be distinguished. The rectangular grid dot pattern is also preferable to utilize  $\mathbf{G}$  and  $\mathbf{C}$  polynomial sets that are introduced in the following paragraphs.

The fiducial dot pattern can be used to systematically quantify the misalignment status when it is associated with vector polynomials. As misalignments shift the image of the fiducial dots from their reference points, we can connect corresponding

dots from their referenced position to their perturbed position to make vectors [Fig. 2(b)].

$\mathbf{G}$  and  $\mathbf{C}$  polynomial sets are vector polynomials derived from the two-dimensional Chebyshev polynomials [15,16]. The  $\mathbf{G}$  polynomial set is derived from the gradients of the two-dimensional Chebyshev polynomials of the first kind, and the  $\mathbf{C}$  polynomial set is based on the curl of two-dimensional Chebyshev polynomials of the first kind. Since both  $\mathbf{G}$  and  $\mathbf{C}$  polynomials are orthogonal sets in the rectangular domain, specific vector terms can be directly related to system errors in alignment of the UUT. While  $\mathbf{G}$  and  $\mathbf{C}$  vector polynomials are utilized in this Letter, the general computational vector fiducial method can be used with any other vector polynomials to be used for different UUT aperture shape applications (e.g., Zernike-based vector polynomials defined over a circular domain).

The reverse optimization algorithm (Eq. 1) is widely used to align optical systems [18,19]:

$$\mathbf{A} = \mathbf{S}\Delta\mathbf{D},$$

$$\mathbf{A} = [a_1 \dots a_i]^T, \quad S_{ij} = \frac{\delta a_i}{\delta x_j}, \quad \Delta\mathbf{D} = \mathbf{x}_j - \mathbf{x}_{jo}. \quad (1)$$

This algorithm consists of three matrices as follows: (1) the measured  $\mathbf{G}$  and  $\mathbf{C}$  polynomial coefficients ( $\mathbf{A}$ ), (2) sensitivity ( $\mathbf{S}$ ), and (3) the amount of misalignment ( $\Delta\mathbf{D}$ ) displacement of each degree of freedom between the current position ( $\mathbf{x}_j$ ) and target position ( $\mathbf{x}_{jo}$ ). Sensitivity means how much the  $\mathbf{G}$  and  $\mathbf{C}$  polynomial coefficients are changed when the system is perturbed by a unit amount in each degree of freedom. The sensitivity can be determined through simulation or actual measurements at each location. After the sensitivity matrix is determined, the misalignment can be calculated using least square fitting from the measured coefficients [Eq. (2)]. This algorithm provides an accurate solution when the sensitivity is linear to the misalignment and the degrees of freedom are orthogonal to each other:

$$\Delta\mathbf{D} = (\mathbf{S}^T \mathbf{S})^{-1} \mathbf{S}^T \mathbf{A}. \quad (2)$$

The performance of the algorithm is verified through simulation and a physical alignment experiment. First the sensitivity was investigated by moving the UUT by a known amount. Random misalignments were then imposed to the UUT's position, and vector data of the fiducial displacements were collected. The set of vector data was then fitted to the  $\mathbf{G}$  and  $\mathbf{C}$  polynomials, and the amount of misalignment was calculated through a reverse optimization process. These processes were repeated until the criteria were met (Fig. 3).

A freeform optic with 2.99 mm peak-to-valley (PV) aspheric departure within a rectangular aperture is used for the simulation study (Fig. 4). During the computational fiducial and its alignment mode generation process, the ideal deflectometry-and-UUT configuration is perturbed and misaligned in the simulation model.

We generated a  $27 \times 20$  grid of 540 dots for vector sampling over the whole UUT aperture for the simulation. The investigated range of sensitivity was  $\pm 0.5$  mm for translations and  $\pm 0.1^\circ$  for tilts. The collected vector data were fitted to 100 terms of each  $\mathbf{G}$  and  $\mathbf{C}$  polynomial. Among the 100 coefficients, we selected the first 22 terms from each  $\mathbf{G}$  and  $\mathbf{C}$  polynomial

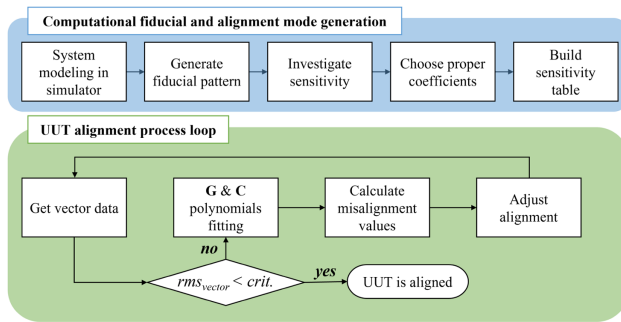


**Fig. 3.** Flowchart of the computational fiducial-based alignment procedure for simulation and physical experiment.

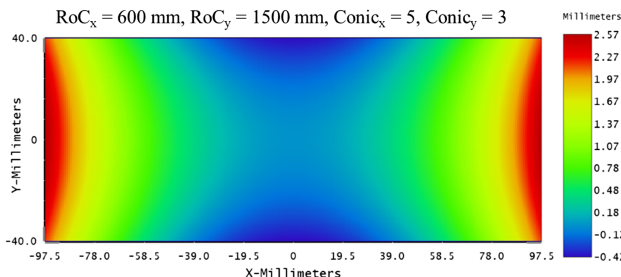


**Fig. 4.** Surface map of sag departure from best-fit sphere for the simulation.

coefficient as the alignment modes, a total of 44 coefficients to build the sensitivity matrix. To calculate the misalignment without degeneracy, each degree of freedom should have distinct sensitivities from one another. Hereafter, translation in  $x$ ,  $y$ , and  $z$  axes are denoted as  $Dx$ ,  $Dy$ , and  $Dz$ , and tilt about  $x$ ,  $y$ , and  $z$  axes are denoted as  $Tx$ ,  $Ty$ , and  $Tz$ , respectively. In general,  $Dx-Ty$  and  $Dy-Tx$  are coupled motions that show similar tendencies. Figure 5 shows the normalized sensitivity ratio of some representative coefficients that have high sensitivities among the used 44 terms. Their sensitivities resemble each other but have different ratios between coefficients to be distinguished as a unique set of alignment mode fingerprints. Considering these characteristics of the sensitivity matrix, we can expect that the misalignments would converge eventually in every degree of freedom with iterations (Fig. 3).

A total of 30 alignment simulations were performed, and the random alignment errors were imposed within the sensitivity investigated range. The alignment end criteria were 0.08 pixel of RMS vector size (0.2  $\mu\text{m}$  in this case) at the image plane. Simulation results are shown in Fig. 6. Although the required

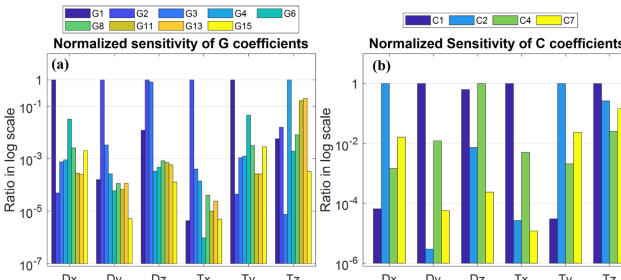


**Fig. 5.** (a) Normalized sensitivity of  $G$  coefficients. (b) Normalized sensitivity of  $C$  coefficients. Both graphs are represented in log scales due to small magnitudes of sensitivities.

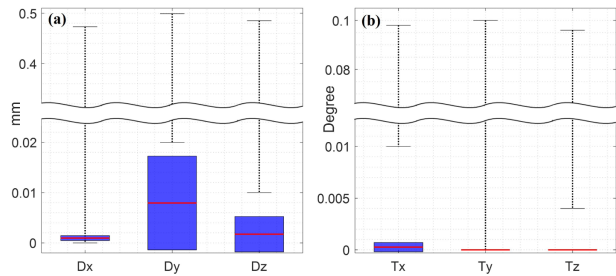


**Fig. 6.** Result of alignment simulation. Dotted lines mean initial random alignment error range, red lines represent mean values of remaining errors, and blue boxes represent standard deviations of each. (a) Translation errors. (b) Tilt errors.

number of alignment steps was varied, the RMS vector sizes were converged and met the criteria at the end. The remaining amounts of misalignments were reasonably small in all 6 deg of freedom. The remaining error for  $Dy$  was relatively higher than others ( $\sim 8 \mu\text{m}$ ), but still within an affordable range to have consistency in surface measurements with deflectometry.

Once the viability of the algorithm had been tested, it was applied to an experimental deflectometry setup (Fig. 1). A 546 mm LCD monitor with  $1920 \times 1080$  resolution was utilized as the light source, and a 3.2 MP camera with a 16 mm focal length objective lens was mounted near the LCD monitor. The UUT we used was a freeform image projection mirror with a rectangular aperture with a width of 195 mm and height of 80 mm.

To track the alignment status precisely, we mounted the UUT on a five-axis motorized stage. (Note: the  $Tx$  was manually fixed due to the limited motorized hardware available in the laboratory.) The as-built vector fiducial alignment hardware system needs to be calibrated because the motion stage hardware, display, and camera are not ideal. It can be calibrated by aligning and measuring a reference UUT. Because the reference surface is known, after the alignment minimizing the surface residual error (i.e., difference between the measured and known surface shapes), the alignment state can be set as the nominal zero state, and the residual error can be calibrated out as systematic error.

Similar to the simulation process, the sensitivity matrix was investigated first. In this case, the UUT was translated  $\pm 0.5$  mm along each axis, and tilted  $\pm 0.1^\circ$  about the  $y$  and  $z$  axes. Then we fit the vector data into 100 terms of each  $G$  and  $C$  polynomial. The total measuring time for  $S$  was about 20 min, yet  $\sim 90\%$  of the time was due to the series of image acquisition periods limited by the as-built motorized stage speed. We built the sensitivity table using the first 20 terms or more from each polynomial, and the alignment criteria were set to less than 0.3 pixel ( $0.75 \mu\text{m}$ ) RMS for the vector size in the detector plane. Then, the random misalignments were imposed within the sensitivity investigated range, and the algorithm was applied to calculate the amount of misalignment. These processes were controlled automatically and calculated repeatedly in closed-loop until alignment criteria were met. A commercial laptop (CPU: i5-1135G7/RAM: 8 GB) was used for calculating and controlling the system, and each iteration took less than 2 min.

A total of 10 alignment experiments were performed, and results are summarized in Fig. 7. The RMS vector size met the criteria, but the remaining amounts of misalignments were various for each degree of freedom.  $Dy$ ,  $Dz$ , and  $Tz$  converged

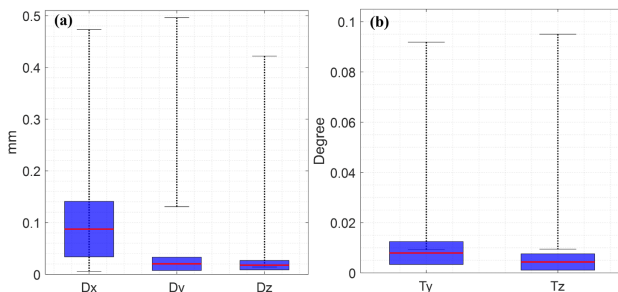


**Fig. 7.** Result of physical experiments. (a) Translation errors. (b) Tilt errors.

well, while Dx and Ty converged as well but had relatively large amounts of errors remaining. This is because Dx and Ty give the similar fiducial motion and are hard to distinguish in vector space.

We highlight that the performance of the alignment status estimation was limited by accuracy of the hardware, not the algorithm itself as long as the misalignment is within a linear range of sensitivity. Indeed, the coupled translation and tilt are already predicted from the simulation stage. As shown in Fig. 5, the translation and tilt motion have distinct behavior in higher order coefficients that are small in magnitude. For this reason, the accuracy of the algorithm can be improved by obtaining more precise vector data or utilizing higher resolution cameras in the deflectometry system. For application of a large misalignment case where misalignments are nonlinear, an adaptive or iteratively updating  $\mathcal{S}$  throughout the alignment process can be applied. Then, updating  $\mathcal{S}$  comes at the cost of modeling or measurement time.

Alignment in most metrology systems is important so that misalignment is not embedded into surface measurements. To validate alignment results, we compared the PV of the subtracted map between a reference surface map and a before/after aligned surface map. The reference is the surface map measured at the home position. Thus the difference map shows both the capability of the alignment loop to bring back the UUT to its original position and repeatability of optical testing. The PV surface map error due to the residual misalignment is less than 8.4  $\mu\text{m}$  in 10 experiments (Fig. 8). The result demonstrated that the proposed computational alignment algorithm can guide deflectometry system alignment to secure repeatability in optical testing without additional alignment devices. This

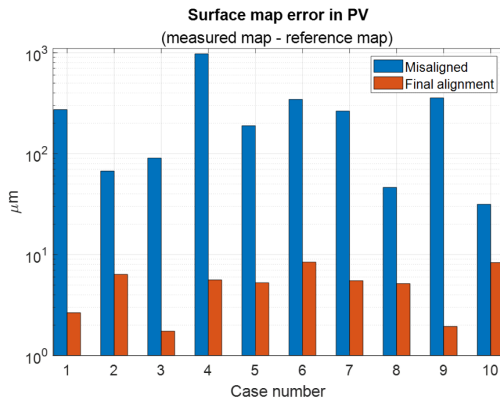


**Fig. 8.** Improvement of surface map matching via alignment loop.

is the deflectometry counterpart of the alignment mode of interferometry.

In conclusion, we have introduced an automatic alignment algorithm for deflectometry systems using computational fiducials and  $\mathbf{G}$ ,  $\mathbf{C}$  vector polynomials. The algorithm is demonstrated through alignment simulation and experiments. In simulation, remaining amounts of displacement were about tens of micrometers in translation and about  $0.001^\circ$  in tilt. In the actual alignment experiment, remaining amounts were slightly higher than simulated due to hardware limitations, but still less than 100  $\mu\text{m}$  in translation and  $0.01^\circ$  in tilt. The optical testing results show only 8.4  $\mu\text{m}$  of maximum difference from the ideal metrology case. These results imply that the proposed algorithm gives a self-calibration and alignment capability to deflectometry that is inevitable for high accuracy testing.

The proposed algorithm provides quick guidelines and accurate solutions in alignment that benefit freeform metrology, especially when rapid and repeated surface measurements are needed in commercial applications such as quality checks for mass production without extra cost or hardware.

**Acknowledgment.** The authors acknowledge the II-VI Foundation Block-Gift Program for helping support general deflectometry research in the LOFT group.

**Disclosures.** The authors declare no conflicts of interest.

**Data Availability.** Data underlying the results presented in this Letter are not publicly available at this time but may be obtained from the authors upon reasonable request.

## REFERENCES

- P. Su, R. E. Parks, L. Wang, R. P. Angel, and J. H. Burge, *Appl. Opt.* **49**, 4404 (2010).
- P. Su, S. Wang, M. Khereishi, Y. Wang, T. Su, P. Zhou, R. E. Parks, K. Law, M. Rascon, T. Zobrist, H. Martin, and J. H. Burge, *Proc. SPIE* **8450**, 340 (2012).
- R. Huang, P. Su, J. H. Burge, L. Huang, and M. Idir, *Opt. Eng.* **54**, 084103 (2015).
- M. Petz and R. Tutsch, *Proc. SPIE* **5869**, 366 (2005).
- Y.-L. Xiao, X. Su, and W. Chen, *Opt. Lett.* **37**, 620 (2012).
- T. Zhou, K. Chen, H. Wei, and Y. Li, *Appl. Opt.* **55**, 7018 (2016).
- X. Deng, N. Gao, and Z. Zhang, *Appl. Sci.* **9**, 1444 (2019).
- M. Hui, X. Li, N. Li, M. Liu, L. Dong, L. Kong, and Y. Zhao, *Meas. Sci. Technol.* **31**, 045010 (2020).
- D. Wang, S. Zhang, R. Wu, C. Y. Huang, H.-N. Cheng, and R. Liang, *Opt. Express* **24**, 19671 (2016).
- D. Wang, Z. Gong, P. Xu, C. Wang, R. Liang, M. Kong, and J. Zhao, *Opt. Express* **26**, 8113 (2018).
- A. Davies, T. Vann, C. Evans, and M. Butkiewicz, *Proc. SPIE* **10373**, 103730H (2017).
- E. Olesch, C. Faber, and G. Häuslerin, in *DGaO Proceedings* (2011), p. 7536.
- X. Xu, X. Zhang, Z. Niu, W. Wang, Y. Zhu, and M. Xu, *Opt. Express* **27**, 7523 (2019).
- C. Wang, N. Chen, and W. Heidrich, *Opt. Express* **29**, 30284 (2021).
- M. Aftab, J. H. Burge, G. A. Smith, L. Graves, C.-J. Oh, and D. W. Kim, *Int. J. Precis. Eng. Manuf. Technol.* **6**, 255 (2019).
- M. Aftab, L. R. Graves, J. H. Burge, G. A. Smith, C. J. Oh, and D. W. Kim, *Opt. Eng.* **58**, 095105 (2019).
- H. Kang, H. Quach, H. Choi, G. A. Smith, and D. W. Kim, *Proc. SPIE* **11487**, 139 (2020).
- H. J. Jeong, G. N. Lawrence, and K. B. Nahm, *Proc. SPIE* **0818**, 430 (1987).
- E. D. Kim, Y.-W. Choi, M.-S. Kang, and S. C. Choi, *J. Opt. Soc. Korea* **9**, 68 (2005).